Geoderma 449 (2024) 117001

Contents lists available at ScienceDirect

Geoderma

journal homepage: www.elsevier.com/locate/geoderma

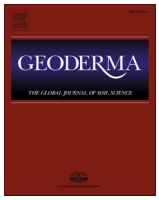

Links between soil pore structure, water flow and solute transport in the topsoil of an arable field: Does soil organic carbon matter?

Jumpei Fukumasu [a,c,*], Nick Jarvis [a], John Koestel [a,b], Mats Larsbo [a]

[a] Department of Soil and Environment, Swedish University of Agricultural Sciences (SLU), Box 7014, 750 07 Uppsala, Sweden
[b] Soil Quality and Soil Use, Agroscope, Reckenholzstrasse 191, Zürich CH-8046, Switzerland
[c] Institute for Agro-Environmental Sciences, National Agriculture and Food Research Organization, Tsukuba 305-8604, Japan

ARTICLE INFO

Handling Editor: Y. Capowiez

Keywords:
Soil pore structure
Soil organic carbon
Preferential transport
X-ray tomography
Macropore

ABSTRACT

An improved understanding of preferential solute transport in soil macropores would enable more reliable predictions of the fate of agrochemicals and the protection of water quality in agricultural landscapes. The objective of this study was to investigate how soil organic carbon (SOC) and soil texture shape soil pore structure and thereby determine the susceptibility to preferential transport under steady-state near-saturated flow conditions. To do so, we took intact topsoil samples from an arable field that has large variations in SOC content (1.1–2.7%) and clay content (8–42%). Soil pore structure was quantified by X-ray tomography and soil water retention measurements. Non-reactive solute transport experiments under steady-state near-saturated conditions were carried out at irrigation rates of 2 and 5 mm h^{-1} to quantify the degree of preferential transport. Near-saturated hydraulic conductivities at pressure heads of −1.3 and −6 cm were also measured using a tension disc infiltrometer. The results showed that larger abundances of small macropores (240–720 μm diameter) and mesopores (5–100 μm diameter) resulted in weaker preferential transport, due to larger hydraulic conductivities in the soil matrix that prevented the activation of water flow and solute transport in large macropores. In particular, the degree of preferential transport was most strongly and negatively correlated with the mesoporosity in the 30–100 μm diameter class. In contrast, the degree of preferential transport was not correlated with connectivity measures (e.g. the percolating fraction and critical pore diameter for the macropore network), probably because i.) the pore space of almost all samples was highly connected, being dominated by one percolating cluster, and ii.) only a part of this percolating macroporosity was active under the near-saturated conditions of the experiment. We also found that the degree of preferential transport was strongly and negatively correlated with clay content, whilst the effects of SOC were not significant. Nevertheless, macroporosity in the 240–720 μm diameter class and mesoporosity were positively correlated with SOC content in our soils and in some previous studies. Therefore, SOC sequestration in arable soils may potentially reduce the risk of preferential transport under near-saturated flow conditions through better developed networks of small macropores and mesopores.

1. Introduction

An improved understanding of the processes of water flow and solute transport in arable soils is important for predicting the fate of agrochemicals and for assessing their consequences for water quality in the surrounding environment. Of particular interest is the occurrence of preferential flow and transport, which can take place when water flows through soil macropores. Through preferential transport, agrochemicals can bypass the soil matrix and be rapidly leached out of the root zone (Jarvis, 2007). This process has been observed experimentally in the field and laboratory and a range of models that account for preferential flow have been developed (Jarvis et al., 2016; Nimmo, 2021).

An improved understanding of the soil pore network properties that regulate the strength of preferential transport may help us to better manage arable soils of diverse properties to limit leaching of agrochemicals and contaminants. The soil porosity in various pore diameter classes can be quantified by measurements of, for example, soil water retention and X-ray tomography (Rabot et al., 2018). Scanning soil samples using X-ray tomography allows quantification not only of macroporosity, but also of many macropore and biopore network

* Corresponding author at: Institute for Agro-Environmental Sciences, National Agriculture and Food Research Organization, Tsukuba, 305-8604, Japan.
E-mail addresses: jumpei.fukumasu@slu.se, jumpei.fukumasu@affrc.go.jp (J. Fukumasu).

https://doi.org/10.1016/j.geoderma.2024.117001
Received 3 May 2024; Received in revised form 24 July 2024; Accepted 9 August 2024
Available online 16 August 2024

characteristics (e.g. connectivity and fractal dimension; Larsbo et al., 2014; Zhang et al., 2019; Lucas et al., 2019). Several studies have investigated links between X-ray derived pore characteristics and water flow. For example, macroporosity (Luo et al., 2010; Schlüter et al., 2019), bioporosity (Zhang et al. 2019), pore connectivity measures (Sandin et al., 2017; Schlüter et al., 2019) and critical pore diameter (Koestel et al., 2018) have been reported to be correlated with near-saturated or saturated hydraulic conductivity. In contrast, fewer studies have investigated the relationships between X-ray derived macropore characteristics and the degree of preferential transport, presumably because solute transport experiments are tedious and expensive. A few previous studies on intact soil columns have reported that the degree of preferential transport was negatively correlated with macroporosity under steady-state near-saturated flow conditions (i.e. preferential transport was weaker for samples with larger macroporosity; Katuwal et al., 2015, Larsbo et al., 2014). In apparent contrast, Paradelo et al. (2016) reported no correlation between imaged macroporosity and the degree of preferential transport. Instead, they found that the degree of preferential transport was strongly and positively correlated with the density of the soil below the image resolution. They suggested therefore that the activation of preferential flow was dependent on the abundance of macropores and mesopores with diameters smaller than the image resolution (<1.2 mm) rather than the characteristics of the networks of larger macropores. With much better image resolution (200 μm), Larsbo et al. (2016) showed that the macroporosity in the 200–600 μm diameter class regulated the degree of preferential transport. These studies suggest that measurements of pore size distributions spanning micro-, meso- and macropores are needed to explain the effects of pore structure on preferential transport. Since macropores are often sparsely distributed, relatively large columns are required for their quantification (Koestel et al., 2020). The trade-off between column size and image resolution means that mesoporosity < ca. 0.3 mm diameter cannot be quantified by standard industrial X-ray tomography on the same samples. Soil water retention measurements can therefore be a useful complement to macropore characteristics obtained by X-ray tomography, even though they only provide estimates of the pore size (diameter) distribution averaged for a whole sample.

Soil pore structure is influenced by basic soil properties such as soil organic carbon (SOC) and clay content (Fukumasu et al., 2022) as they directly and indirectly affect several biological and physical processes that lead to soil aggregation and the formation of macropores (Horn et al., 1994, Dexter et al., 2008, Meurer et al., 2020a). It is well established from both field and laboratory studies that the risk of preferential transport is generally larger in clay soils compared to soils with coarser texture (e.g. Ghafoor et al. 2012; Karup et al., 2016; Sandin et al., 2018; Demand et al., 2019). However, relationships between water flow and solute transport and SOC content are less clear. A better understanding of these relationships is important, since sequestration of SOC in agricultural soil has gained attention as a promising strategy to improve soil physical quality and mitigate climate change (Johannes et al., 2017; Chenu et al., 2019; Fu et al., 2021). Only a few studies have investigated the effects of SOC on preferential transport. These studies suggest that the typical spatial variation in SOC contents at the field scale may not be large enough to quantify its effect on preferential transport. For example, Vendelboe et al. (2013) and Soares et al. (2015) reported no effects of SOC on the degree of preferential transport for samples with SOC variations of 1.2–1.7% and 1.7–2.2% respectively. On the other hand, Larsbo et al. (2016) and Paradelo et al. (2016) reported that larger SOC content was associated with a lower risk of preferential transport for soils with SOC contents in the ranges 4–15% and 1.8–8.4%, respectively. Ideally, these relationships should be assessed for the typical range of SOC contents found in arable topsoil. In arable soils, the SOC content is typically smaller than 3% (Oldfield et al., 2019). For example, SOC content is smaller than 3.5% for 75% of the samples in the Swedish national inventory of arable topsoils (Eriksson et al., 2010).

The objective of this study was to investigate how the degree of preferential transport estimated from non-reactive solute breakthrough curves is influenced by basic soil properties (SOC and clay content), soil pore size distribution estimated from water retention curves and pore network characteristics quantified by X-ray tomography. We examined these relationships statistically in an attempt to improve our understanding of preferential solute transport in arable topsoils with diverse pore characteristics. Specifically, we tested the hypothesis that in the typical range of SOC contents of Swedish arable topsoils (i.e. <3%), the degree of preferential transport should decrease with higher SOC content as it should promote the development of well-connected networks of mesopores and smaller macropores (Fukumasu et al., 2022), which should prevent water flow in larger macropores. These measurements were made on samples taken from a conventionally-tilled arable field with large variations in SOC content (1.1–2.7%) and clay content (8–42%) where the management across the field had been similar for about 60 years, which should have minimized the effects of confounding factors (e.g. climate and soil management) on soil structure.

2. Materials and methods

2.1. Field description and soil sampling

The field (46.9 ha) is located in Bjertorp in central-western Sweden (58°14′00″N 13°08′00″E). A more detailed site description is available in Fukumasu et al. (2021). Briefly, the field has been cultivated for at least 60 years mainly with oats, oilseed rape and winter wheat. The land management has been similar across the field except that different crop varieties were grown in some parts in some years and precision fertilization of nitrogen, phosphorus and potassium was performed in some years. The mean annual temperature and precipitation were 7.3 °C and 624 mm, respectively. Soil profiles dug at three locations within the field were classified as Stagnic Eutric Cambisol, Eutric Stagnosol and Haplic Phaeozem. In late August 2017, after the harvest of oilseed rape but before tillage, we conducted soil sampling at 35 locations selected using stratified sampling to cover wide ranges in clay (8–42%) and SOC (1.1–2.7%) contents. At each location, we took (1) intact soil in polyvinyl chloride (PVC) cylinders (20 cm high, 12.5 cm inner diameter) at a depth starting from the soil surface to ca. 17 cm, (2) intact soil in steel cylinders (10 cm high, 6.8 cm inner diameter) at a depth from ca. 3–13 cm and (3) loose soil at a depth from ca. 3–13 cm. The three samples were taken as close to each other as possible (i.e. within ca. 30 cm) at each sampling location. The PVC cylinder samples were used for X-ray scanning, solute transport experiments and near-saturated hydraulic conductivity measurements. After these experiments, soil was extracted from the PVC cylinders at depths of between ca. 3 to 13 cm. This soil was then air-dried, sieved to <2 mm and used for soil texture and SOC analyses. The soil samples in the steel cylinders were used for measurements of soil water retention and bulk density. The loose soils were also air-dried, sieved to <2 mm and used for measurements of water content at wilting point.

2.2. Soil properties and soil water retention

Soil texture was determined by wet-sieving and the pipette method. In this analysis, soil samples were dispersed by removal of soil organic matter using a peroxide solution (35 %) and by addition of a chemical dispersant (7 g/L sodium carbonate, Na2CO3 + 33 g/L sodium metaphosphate, (NaO3P)n). SOC content was measured by dry-combustion on a TruMac CN (LECO Corp.). In a previous study we confirmed that the inorganic carbon content was negligible (Fukumasu et al., 2021). Soil water retention was measured at pressure potentials of −30, −100, −300, − 600 and −15000 cm (Fukumasu et al., 2022). We converted each pressure potential (ψ) to an equivalent pore diameter (d, (μm)) using the Young-Laplace equation: $d = -3000/\psi$. By calculating differences in volumetric water contents between pressure potentials, we estimated porosities in different pore diameter classes (<0.2 μm, 0.2–5

μm, 5–10 μm, 10–30 μm, 30–100 μm and >100 μm). Total porosity was estimated from bulk density assuming a particle density of 2.65 g cm^{-3}. Statistical summaries of soil properties and pore size distributions are given in Tables S1 and S2.

2.3. X-ray tomography

The large intact soil columns were scanned using the GE Phoenix X-ray scanner (v|tome|x 240) available at the Department of Soil and Environment at the Swedish University of Agricultural Sciences, Uppsala. The tomography settings are given in Fukumasu et al. (2022). The voxel edge length in the resulting 3D images was 120 μm. A centrally located cylindrical region of interest with a diameter of 8.4 cm was chosen at the 3.0–13.0 cm depth so that any artificial pores created at sampling close to the column walls were excluded. The location of the soil surface was defined as the depth where the fraction of voxels classified as solids exceeded 50 % (Larsbo et al., 2014).

2.4. Image processing and analysis

Image processing and analysis were carried out using the FIJI distribution (Schindelin et al., 2012) of the open-source software ImageJ and the plugin SoilJ (Koestel, 2018). Details of the image processing are given in Fukumasu et al. (2022). From the resulting binary images we calculated total visible porosity and macropore network characteristics using SoilJ (Koestel, 2018). Porosity in different pore diameter classes were derived using pore thickness images and a histogram tool in ImageJ. In this study we included the specific surface area of macropores (SSA, mm^2 mm^{-3}), average macropore thickness (Th, mm), surface fractal dimension (D_s, dimensionless), connection probability (Γ, dimensionless), critical pore diameter ($d_{critical}$ (mm)) and the percolating fraction (PF, dimensionless). The fractal dimension is a measure of how the macropore surface area increases with decreasing image voxel size, i.e. with the decrease of the measuring unit used. Large fractal dimensions indicate larger fractions of smaller macropores and a larger roughness of larger macropores such that more spaces are filled with pores in a given volume. The connection probability is the probability that two randomly selected pore voxels belong to the same pore cluster, while the percolating fraction is the fraction of the pore network that is connected to the top and the bottom of the ROI (Renard and Allard, 2013; Jarvis et al., 2017a). The critical pore diameter reflecting the bottleneck diameter on the percolating cluster is derived from the diameter of the largest sphere that can pass through the sample from top to bottom (Koestel et al., 2018). Additionally, biopores defined as all tubular pores were identified using a method based on Lucas et al. (2019). For these calculations we first reduced the resolution of the original images by a factor of two to reduce computation time. Details of the method are given in Fukumasu et al. (2022). We then calculated total bioporosity using SoilJ and biopore size distributions using thickness images and a histogram tool. Both macropores and biopores were divided into the following pore diameter classes: 240–480, 480–720, 720–1220, 1220–1920, 1920–3120 and >3120 μm. For this we did not include the upper limit of diameter in each pore size class (e.g. $480 \leq Ø < 720$ μm). For biopores, the smallest diameter class was not included because of the reduced resolution. Statistical summaries of the macropore size distributions and biopore size distributions are given in Tables S3 and S4. Additionally, to examine the connectivity of only the small macropores ($240 \leq Ø < 480$ μm), the original thickness images were segmented by applying a given threshold to isolate the small macropores. We then analyzed the network characteristics of small macropores using SoilJ.

2.5. Solute transport experiments

Solute transport experiments were conducted under steady-state water flow following the method described in Larsbo et al. (2014, 2016). Briefly, prior to the irrigation experiment, polyamide cloths with 50 μm mesh size were attached to the bottom of the PVC cylinders to prevent soil loss during the experiment. The soil samples were irrigated with artificial rainwater at 2 mm h^{-1} intensity for about 5 days to flush out solutes from the soil and thereby stabilize solute concentrations in effluents collected from the bottom. A pulse of 2 mL potassium bromide (250 mg Br mL^{-1} distilled water) was then applied to the soil surface within ca. 90 s. This application was restricted to a centrally located area ca. 10 cm in diameter on the surface to limit solute flow through any artificial pores located close to the cylinder walls. The electrical conductivity of the effluent was measured at 5 min resolution using a Cond 3310 (WTW GmbH, Weilheim, Germany) to obtain tracer breakthrough curves. The weights of the effluents were measured daily to verify that the irrigation intensity was constant. After the first breakthrough experiment, the irrigation intensity was increased to 5 mm h^{-1}. A pulse of 2 mL potassium bromide was again applied to the soil surface and breakthrough curves of the solutes in effluents were recorded. In this experiment, we assumed a linear relationship between bromide concentration and electrical conductivity (CRC Handbook of Chemistry and Physics, 1989). The samples that had ponding water on the soil surface as well as samples exposed to variable irrigation intensities during the experiments were removed from the dataset to ensure consistent boundary conditions among the samples. The final dataset consisted of 33 and 26 samples for the 2 mm h^{-1} and 5 mm h^{-1} irrigation intensities, respectively.

In the present study, we used the normalized 5% arrival time estimated from the breakthrough curves as an indicator for the degree of preferential transport (Knudby and Carrera, 2005; Koestel et al., 2011), where early arrival (i.e. small values for the 5% arrival time) of the applied solute indicates stronger preferential transport. Details on the calculation of normalized 5% arrival times is described in Larsbo et al. (2014). For this calculation, we subtracted the "background" electrical conductivity in the effluent solution (i.e. resident ions in soil solution), which was derived from curve-fitting during the electrical conductivity in the entire irrigation period, from the original electrical conductivity (Fig. S1; Larsbo et al., 2014). We also used dimensionless time, obtained by dividing the time since KBr application by the average arrival time calculated from zeroth and first moments (Larsbo et al., 2014).

2.6. Near-saturated hydraulic conductivity

After the irrigation experiment, near-saturated hydraulic conductivity was measured on the soils in the PVC cylinders using a tension disc infiltrometer. Before these measurements, soil samples inside the PVC cylinders were pushed up a few centimeters from the bottom so that the infiltrometer could be placed on the soil surface. The bottom of the samples was filled with fine sand. The surfaces of the soil samples were gently evened out with the tip of a knife and a ca. 0.5 cm thick layer of fine sand was then added to allow for good contact between the infiltrometer disc and the soil. It was not possible to make measurements for one sample having the largest clay content (42%) due to significant smearing of the soil surface during sample preparation. Steady-state infiltration rates were measured at two supply pressure potentials, first at −6 and then at −1.3 cm (equivalent to nominal maximum conducting pore diameters of 0.5 and 2.3 mm, respectively). Given the approximately one-dimensional flow, infiltration rates were considered to be equivalent to hydraulic conductivities. These measurements were used to estimate the diameter of the largest water-filled pore during the irrigation experiment, by assuming a linear relation between log-transformed pressure potentials and log-transformed near-saturated hydraulic conductivities close to saturation (Jarvis et al., 2013; Larsbo et al., 2014). The degree of saturation in macropores was calculated using the diameter of the largest water-filled pore and X-ray derived macropore size distributions. For the fitting of macropore size distribution, we used a log-normal model (Kosugi, 1994) to derive the median and standard deviation of the macropore size distribution.

2.7. Statistical analysis

We determined correlation coefficients for relationships between 5% arrival times, near-saturated hydraulic conductivities, the diameters of the largest water-filled pore during the solute transport experiments, soil pore characteristics and soil properties. We used Spearman rank correlation coefficients because some of these variables were not normally distributed. Relationships with relatively high correlation coefficients are also shown graphically. Regression analysis was conducted to determine the extent to which soil pore characteristics could explain the variation in 5% arrival times. We used $P<0.05$ as the significance level.

3. Results

3.1. X-ray derived macropore characteristics and their relation to pore size distributions and soil properties

Large variations in the X-ray derived macropore network characteristics among the soil samples were found (Table S5). For example, the ranges of specific surface area and connection probability were 0.21–0.95 mm^2 mm^{-3} and 0.58–0.96 (−), respectively. All characteristics were correlated to X-ray derived macroporosities for most diameter classes (Fig. 1). The specific surface area of macropores and the surface fractal dimension were most strongly and positively correlated with porosity in the 240–1200 μm diameter classes (Fig. 1). Macropore networks were percolating (i.e. connected from top to bottom) for 34 out of 35 samples. The connection probability and percolating fraction were positively correlated with macroporosity in all classes, while the critical pore diameter was positively correlated with macroporosity in ≥720 μm diameter classes (Fig. 1). The connection probability and the percolating fraction were strongly correlated with total visible porosity ($\rho = 0.94$ and $\rho = 0.94$, Fig. 2a,b) and with each other (Fig. 2c). Additionally, the analysis of the connectivity of small macropores (i.e. the 240–480 μm diameter class, with macropores ≥480 μm diameter removed) showed that 33 out of 35 samples had a connection probability smaller than 0.01 and none of the pore networks of this size range in the samples were percolating.

Regarding the effects of soil properties on the macropore characteristics, surface fractal dimension was negatively correlated with clay content, while it was positively correlated with SOC content (Fig. 3). The other X-ray derived characteristics were not correlated with soil properties except for the specific surface area, which was positively correlated with SOC content, the average pore thickness, which was positively correlated with silt content and the critical pore diameter which was positively correlated with clay and silt content (Fig. 3).

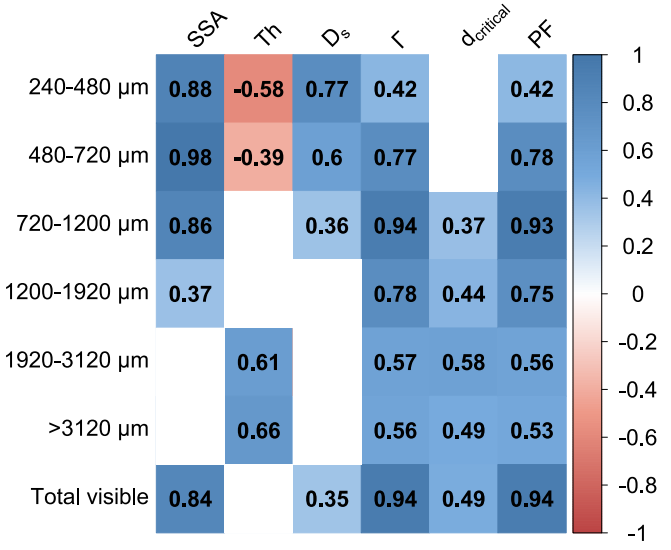

Fig. 1. Correlation matrix for X-ray derived pore size classes and macropore characteristics. Significant correlations ($P<0.05$) are highlighted either in red (negative) or in blue (positive). SSA: specific surface area of macropores; Th: average macropore thickness; D_s: surface fractal dimension; Γ: connection probability; $d_{critical}$: critical pore diameter; PF: percolating fraction. (For interpretation of the references to colour in this figure legend, the reader is referred to the web version of this article.)

3.2. The degree of preferential transport and its relation to the diameter of the largest water-filled pore and the degree of saturation in macropores

Examples of three breakthrough curves with contrasting normalized 5% arrival times are shown in Fig. 4. Large variations in normalized 5% arrival were found among the samples (Table S6), while its mean value decreased from 0.39 to 0.26 with an increase in irrigation intensity from 2 mm h^{-1} to 5 mm h^{-1}. The diameters of the largest water-filled pore during the solute transport experiment varied between 0.02 and 0.33 cm and 0.03 and 0.32 cm for the 2 and 5 mm h^{-1} irrigation intensities, respectively (Table S6). The 5% arrival times were negatively correlated with the diameter of the largest water-filled pore and the estimated degree of saturation in macropores at both irrigation intensities (Fig. 5a and b).

3.3. Effects of X-ray derived macropore characteristics on near-saturated hydraulic conductivities and the degree of preferential transport

Near-saturated hydraulic conductivities and 5% arrival times were positively correlated with the surface fractal dimension (Fig. 6). The 5% arrival time at an irrigation intensity of 2 mm h^{-1} was also positively correlated with specific surface area. On the other hand, hydraulic conductivity and 5% arrival times were not correlated with the connectivity of the macropore networks (i.e. the connection probability and percolating fraction). Regression analysis showed that the surface fractal dimension explained 65% (2 mm h^{-1}) and 53% (5 mm h^{-1}) of the variation in 5% arrival times (Fig. 7).

3.4. Effects of X-ray derived macroporosity in different pore diameter classes on the degree of preferential transport

The 5% arrival times, near-saturated hydraulic conductivities, and diameters of the largest water-filled pores and X-ray derived pore size distributions were correlated with macroporosity in pore size classes smaller than 720 μm (Fig. S2). The 5% arrival times were negatively correlated with bioporosity in 720–1920 pore size classes, whereas these variables were not correlated with bioporosity in larger macroporosity (Fig. S3). The relatively strong relationships between 5% arrival times and porosities in the 240–1920 μm diameter classes are shown in Fig. 8. The linear regression analysis presented in Fig. 8 also shows that the 5% arrival time for the 2 mm h^{-1} irrigation rate was best explained by the porosity in the 240–480 μm diameter class ($R^2 = 37\%$), whereas the 5% arrival time for the 5 mm h^{-1} irrigation rate was best explained by the bioporosity in the 1200–1920 μm diameter class ($R^2 = 40\%$).

3.5. Effects of pore size distributions derived from soil water retention measurements on the degree of preferential transport and near-saturated hydraulic conductivities

Five percent arrival times and near-saturated hydraulic conductivities were positively correlated with the porosity in the 5–100 μm diameter classes, while the diameters of the largest water-filled pores were negatively correlated with these porosities (Fig. S4). In particular, the 5 % arrival times were most strongly correlated with the porosity in the 30 – 100 μm diameter class compared with 5–10 and 10–30 μm diameter classes (Fig. 9). The regression analysis showed that 62% (2 mm h^{-1}) and 70% (5 mm h^{-1}) of the variations in 5% arrival times were explained by the log-transformed porosity in the 30–100 μm diameter class (Fig. 9c).

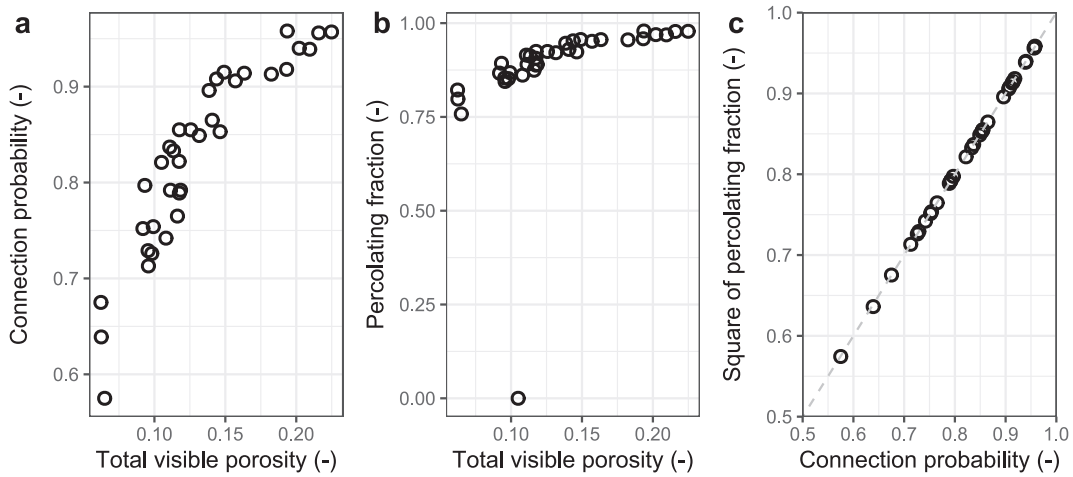

Fig. 2. Relationships between (a) total visible porosity and connection probability (b) total visible porosity and percolating fraction, and (c) square of percolating fraction and connection probability. Note that for (c) 1:1 dashed line is shown in gray and one sample that does not percolate is not shown.

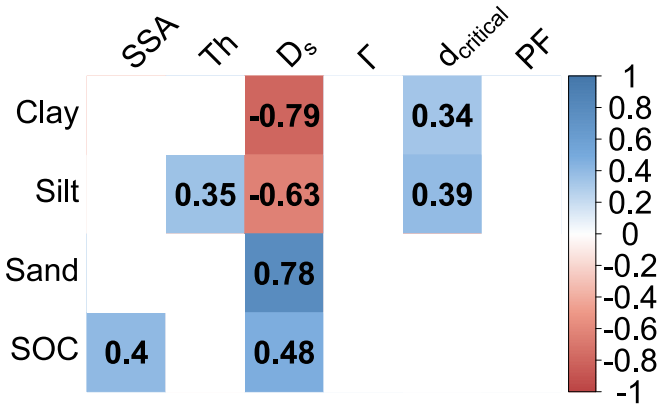

Fig. 3. Correlation matrix for X-ray derived macropore characteristics and soil properties. Significant correlations ($P < 0.05$) are highlighted either in red (negative) or in blue (positive). SSA: specific surface area of macropores; Th: average macropore thickness; D_s: surface fractal dimension; Γ: connection probability; $d_{critical}$: critical pore diameter; PF: percolating fraction. (For interpretation of the references to colour in this figure legend, the reader is referred to the web version of this article.)

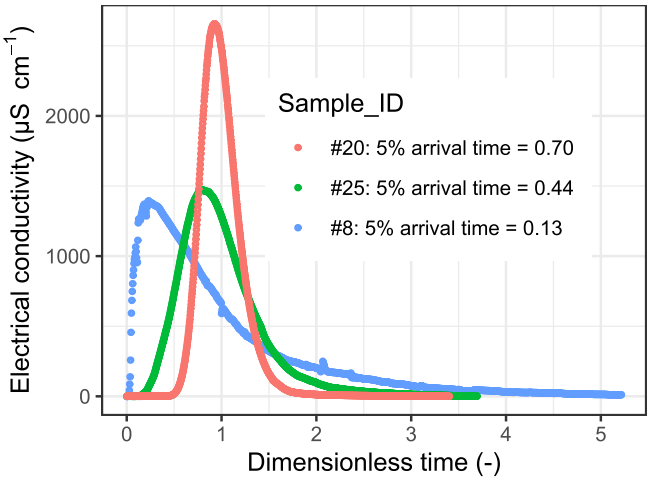

Fig. 4. Examples of three breakthrough curves with contrasting normalized 5% arrival times under 2 mm h^{-1} irrigation intensity. The dimensionless time was obtained by dividing the time since the KBr application by the average arrival time calculated from the zeroth and first moments of the breakthrough curve. The electrical conductivity was corrected for "background" electrical conductivity (see also Fig. S1).

3.6. Relationships between soil properties, water flow and solute transport and the degree of preferential transport

Five percent arrival times and near-saturated hydraulic conductivities were negatively correlated with clay content, while the diameters of the largest water-filled pores and the degree of saturation in macropores were positively correlated with clay content (Fig. 10). The near-saturated hydraulic conductivity at −6 cm pressure potential was positively but weakly correlated with SOC content, whereas the remaining variables were not significantly correlated with SOC (Fig. 10).

4. Discussion

4.1. Effects of macropore characteristics on the degree of preferential transport

The total visible porosities in our samples (0.062–0.225) were large compared to X-ray imaged porosities for Swedish arable soils previously reported (Jarvis et al., 2017a,b; Larsbo et al., 2014) with the exception of those reported by Casali et al. (2024). This large total visible porosity resulted in highly connected imaged pore networks (Fig. 2 and Table S5). All the samples except one of the sandy soils (>65% sand content) had percolating imaged pore networks connecting the top and bottom of the ROI, while the square of percolating fraction was equivalent to the connection probability (i.e. all data points of percolating samples fell on the 1:1 line, Fig. 2c). These results indicate that the imaged porosity in all cases but one was dominated by one percolating cluster (Jarvis et al., 2017a). This may be one reason why there were no significant correlations between 5% arrival times or hydraulic conductivities and the pore connectivity measures included in this study, as we only expect a strong impact of macropore connectivity on preferential transport at or close to the percolation threshold (Larsbo et al., 2014). Another plausible reason is that the connectivity measures were calculated for the whole macropore network, while only part of this network was water-filled and, hence, active in the near-saturated flow conditions of our experiment (Mori et al., 1999; Sammartino et al., 2015). Our results showed that the average degree of saturation in macropores was 48% at 2 mm h^{-1} intensity and 61% at 5 mm h^{-1} intensity and that many of the samples had a degree of saturation much smaller than 50% (Fig. 5b).

The surface fractal dimension emerged as an important X-ray derived

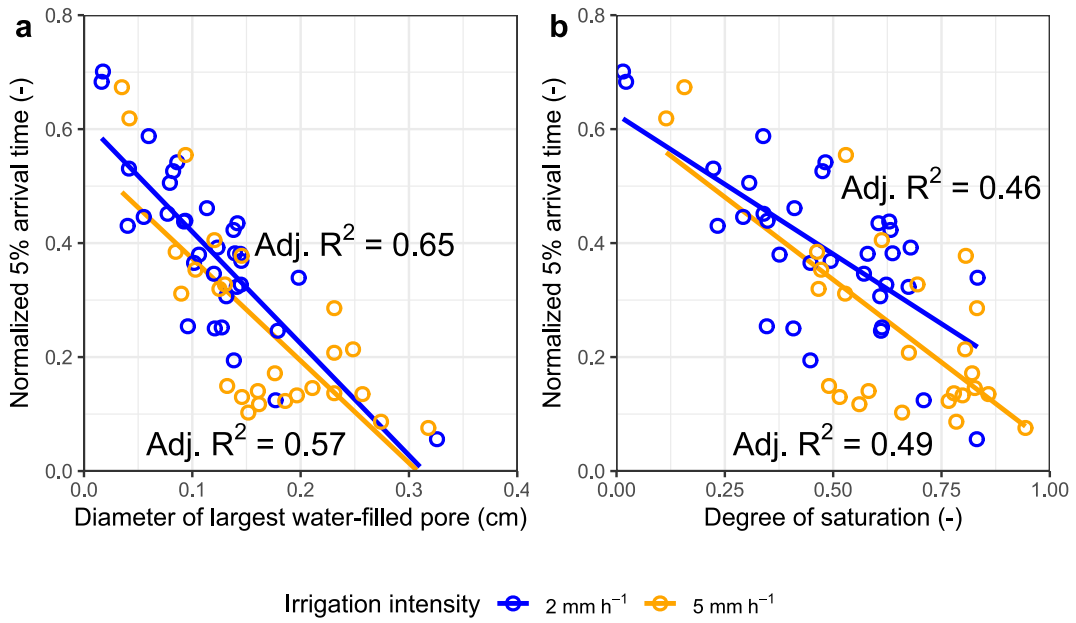

Fig. 5. Relationships between normalized 5% arrival time and (a) diameter of the largest water-filled pore (cm) and (b) the degree of saturation in macropores. The linear regression lines with adjusted R^2 values are displayed when the relationship was significant ($P < 0.05$). Circles in blue and yellow represent the results under irrigation intensity of 2 mm h^{-1} and 5 mm h^{-1}, respectively. (For interpretation of the references to colour in this figure legend, the reader is referred to the web version of this article.)

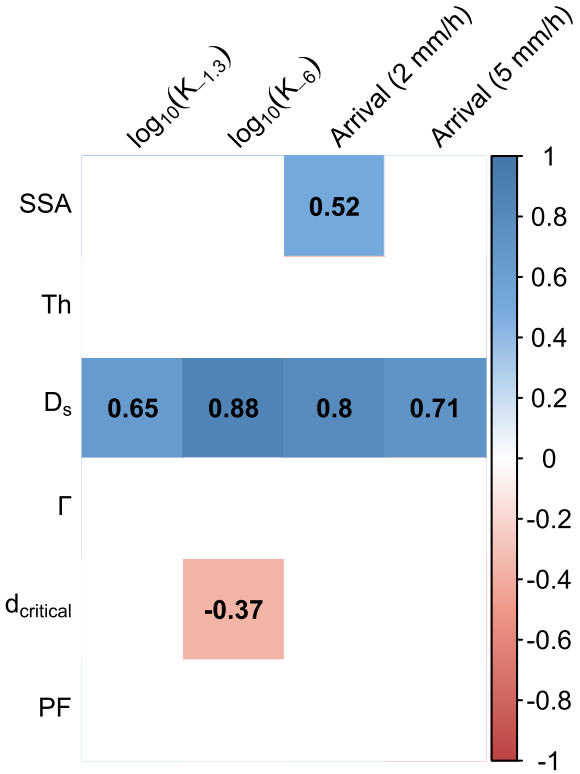

Fig. 6. Correlation matrix for log-transformed hydraulic conductivity (K; −1.3 cm and −6 cm), normalized 5% arrival time (Arrival; 2 mm h^{-1} and 5 mm h^{-1} irrigation intensity) and X-ray derived macropore characteristics. Significant correlations ($P < 0.05$) are highlighted either in red (negative) or in blue (positive). SSA: specific surface area of macropores; Th: average macropore thickness; D_s: fractal dimension; Γ: connection probability; $d_{critical}$: critical pore diameter; PF: percolating fraction. (For interpretation of the references to colour in this figure legend, the reader is referred to the web version of this article.)

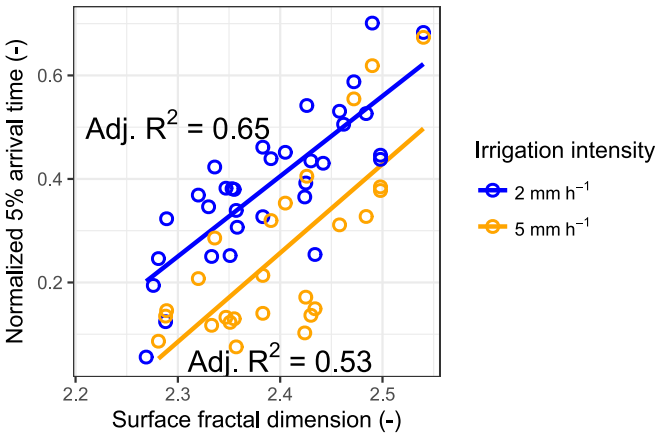

Fig. 7. Relationships between normalized 5% arrival time and surface fractal dimension. The linear regression lines with adjusted R^2 values are displayed when the relationship was significant ($P < 0.05$). Circles in blue and yellow represent the results under irrigation intensity of 2 mm h^{-1} and 5 mm h^{-1}, respectively. (For interpretation of the references to colour in this figure legend, the reader is referred to the web version of this article.)

macropore network characteristic for explaining the variations in the 5% arrival times. Positive correlations between fractal dimension and 5% arrival times have been previously reported by Larsbo et al. (2014, 2016). These results stress the importance of the fraction of small macropores and their spatial distribution for the activation of preferential transport. Generally, smaller macropores and mesopores are more uniformly distributed than larger macropores (Jarvis, 2007; Koestel et al., 2020). This was also evident in our data, which showed a strong positive correlation between surface fractal dimension and porosity in the 240–720 μm diameter class, while the surface fractal dimension was only weakly or not correlated with porosities in larger diameter classes (Fig. 1). To illustrate spatial distribution of small macropores within an ROI, examples of 3D images of pores in 240–480 μm size class in our samples are shown in Fig. 11. Samples #8 and #14 have contrasting clay

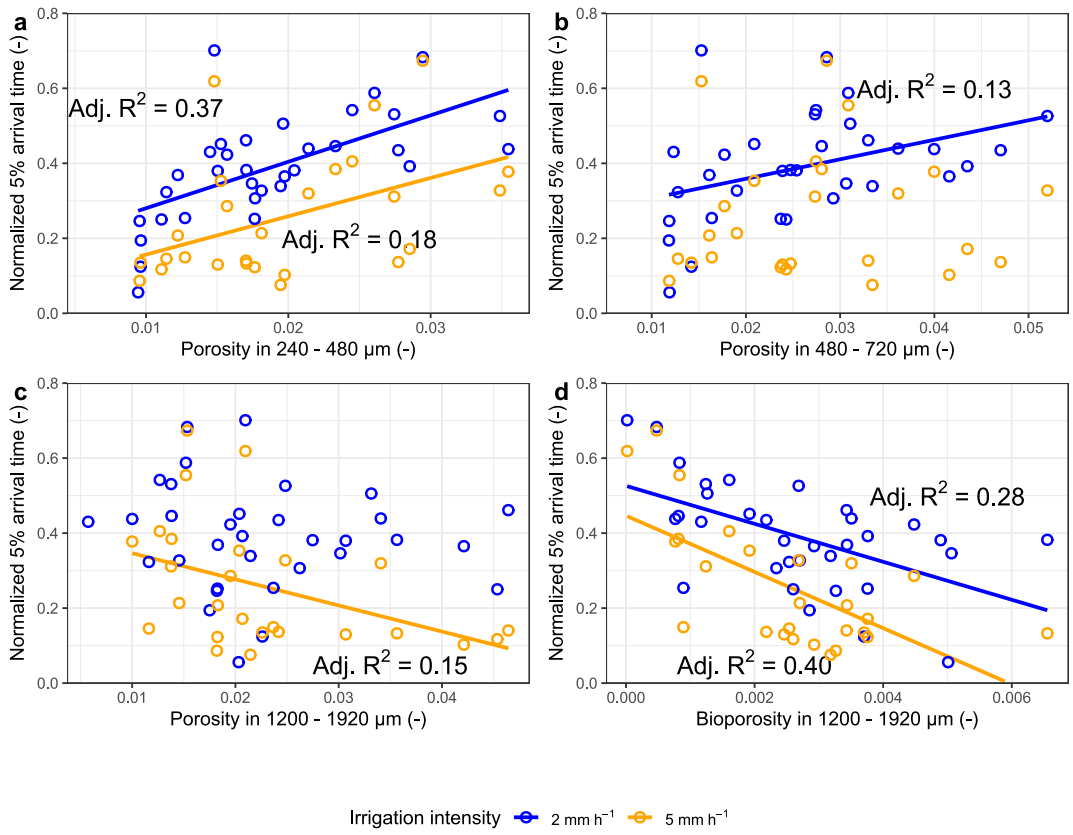

Fig. 8. Relationships between normalized 5% arrival time and (a) X-ray derived porosity in the 240–480 µm diameter class, (b) X-ray derived porosity in the 480–720 µm diameter class, (c) X-ray derived porosity in the 1200–1920 µm diameter class and (d) X-ray derived bioporosity in the 1200–1920 µm diameter class. The linear regression lines with adjusted R^2 values are displayed when the relationship was significant ($P < 0.05$). Circles in blue and yellow represent the results under irrigation intensity of 2 mm h^{-1} and 5 mm h^{-1}, respectively. (For interpretation of the references to colour in this figure legend, the reader is referred to the web version of this article.)

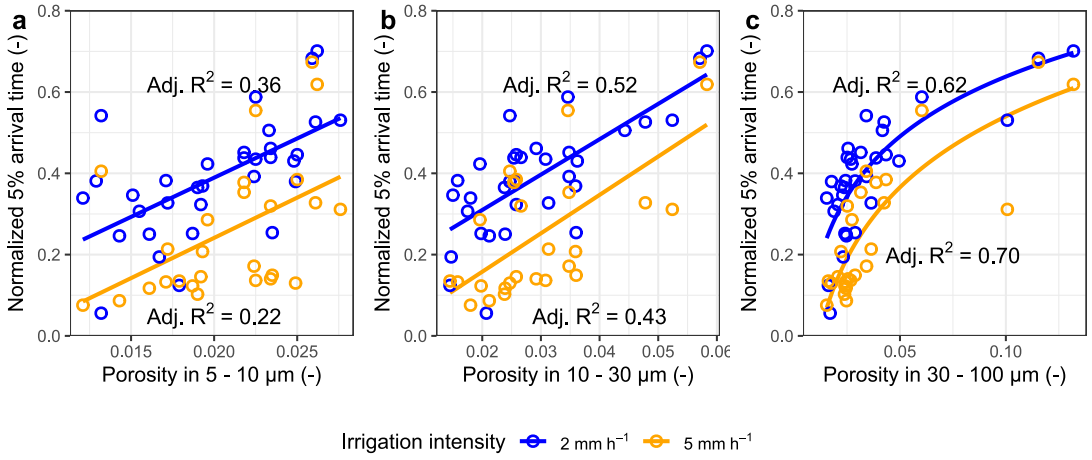

Fig. 9. Relationships between normalized 5% arrival time and (a) porosity in the 5–10 µm diameter class, (b) porosity in the 10–30 µm diameter class and (c) porosity in the 30–100 µm diameter class. The porosities were derived from soil water retention measurements. The regression lines with adjusted R^2 values are displayed when the relationship was significant ($P < 0.05$). Circles in blue and yellow represent the results under irrigation intensity of 2 mm h^{-1} and 5 mm h^{-1}, respectively. (For interpretation of the references to colour in this figure legend, the reader is referred to the web version of this article.)

contents (41.7% vs. 9.8%), while their SOC contents are similar (1.1% vs. 1.3%). Samples #12 and #35 have contrasting SOC contents (1.5% vs. 2.7%), whereas their clay contents are similar (19.1% vs. 21.8%). As clearly shown in these images, the surface fractal dimension was affected strongly by clay content and weakly by SOC content (Fig. 3).

4.2. Pore size distributions and preferential transport

The 5 % arrival times were generally positively correlated with the porosities of small macropores and mesopores, both quantified by X-ray tomography (240–720 µm diameter class) and estimated by soil water retention (5–100 µm diameter classes), while they were generally not correlated with the macroporosity for pore diameters larger than 720 µm

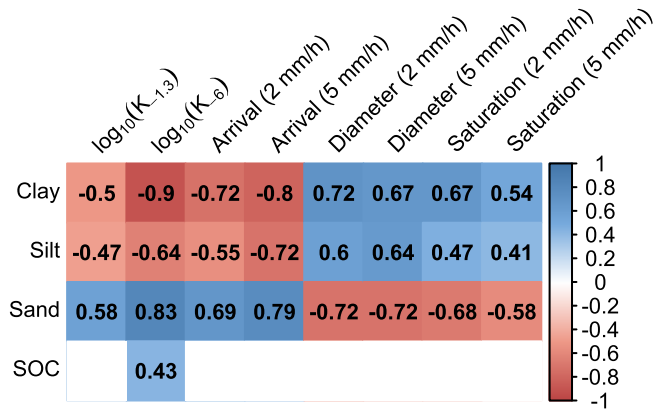

Fig. 10. Correlation matrix for log-transformed hydraulic conductivity (K; −1.3 cm and −6 cm), normalized 5% arrival time (Arrival; 2 mm h^{-1} and 5 mm h^{-1} irrigation intensity), diameter of the largest water-filled pore (Diameter; 2 mm h^{-1} and 5 mm h^{-1} irrigation intensity), the degree of saturation in macropores (Saturation; 2 mm h^{-1} and 5 mm h^{-1} irrigation intensity) and soil properties. Significant correlations ($P < 0.05$) are highlighted either in red (negative) or in blue (positive). (For interpretation of the references to colour in this figure legend, the reader is referred to the web version of this article.)

in our experimental condition. This is consistent with results presented in Larsbo et al. (2016) who reported that the porosity in the 200–600 μm diameter class was a strong predictor for 5% arrival times under steady-state near-saturated flow conditions similar to this study. The negative correlations between these porosities and the diameters of the largest water-filled pore (Fig. S2 and S4) indicate that the small macropores and mesopores controlled the hydraulic conductivity in soil matrix, the activation of flow in larger macropores and, thereby, preferential transport. This is in line with the conceptual models proposed by Jarvis et al. (2012) and Larsbo et al. (2014). Another noticeable point is that the porosity in the 30–100 μm diameter class is a stronger predictor for 5% arrival times than the X-ray derived macroporosities. A plausible explanation for this is that the mesoporosity estimated from soil water retention may better reflect the pores that were actively transporting water (Rabot et al., 2018; Vogel, 2000). Additionally, the analysis of connectivity of only the small macropores (240–480 μm diameter class) illustrated in Fig. 11 showed that these small macropores themselves were poorly connected with one another and, hence, needed to be connected by smaller sized pores, most likely mesopores in the 30–100 μm diameter class, to contribute to water flow. This may also explain why the near-saturated hydraulic conductivity at −6 cm pressure potential was more strongly correlated with the mesoporosity than the small macroporosity (Fig. S2 and S4). It should also be noted that the porosity in the 30–100 μm diameter class was two times larger than that in the 240–480 μm diameter class (Tables S2 and S3). The importance of pores with diameters <100 μm in preventing preferential flow is consistent with previous studies. For example, Langner et al. (1999) conducted solute transport experiments under various controlled pressure potentials and reported that pores smaller than 300 μm diameter did not contribute to preferential flow. Mori and Higashi (2009) also reported that the activation of preferential transport in an Andisol was prevented when a −3 kPa pressure potential (corresponding to 100 μm pore diameter) was applied to the bottom of the soil samples. In addition to controlling the activation of larger pores, mesopores (5–100 μm diameter) would also have a larger surface area in relation to pore volume compared with macropores. The mesopores should therefore facilitate diffusion of solutes into smaller pores (Koestel and Larsbo, 2014). This efficient mass exchange with micropores (<5 μm in diameter) should also reduce the degree of preferential transport (Jarvis, 2007).

The average diameter of the largest water-filled pore increased from 1.1 to 1.6 mm when the irrigation intensity increased from 2 to 5 mm h^{-1}. At this larger flow rate, where a larger fraction of large pores were water filled, 5% arrival times were negatively correlated with imaged macroporosity in the 1200–3120 μm diameter class and with bioporosity in the 1200–1920 μm diameter class. This suggests that the abundance of these larger macropores increases the degree of preferential transport, once flow in them is triggered.

4.3. Soil properties and solute transport: Does SOC matter?

The 5% arrival times were strongly and negatively correlated with clay content whereas they were not correlated with SOC content ($\rho = 0.32$, $P = 0.07$ and $\rho = 0.30$, $P = 0.14$ for 2 mm h^{-1} and 5 mm h^{-1} irrigation intensities, respectively), which indicates that the effect of SOC on preferential transport was limited in this field. We also conducted multiple linear regression analysis using SOC and clay contents as predictors for 5% arrival times, which showed that SOC was not a significant predictor. These results are in line with results at the small-catchment scale in Sweden (Ghafoor et al., 2012), at the national scale in Denmark (Karup et al., 2016) and from a global *meta*-analysis (Koestel et al., 2012). These studies all reported limited effects of SOC on normalized 5% arrival times and found much stronger effects of soil texture. Nevertheless, larger SOC contents may reduce the degree of preferential transport through its association with smaller macropores and mesopores (Larsbo et al., 2016; Paradelo et al., 2016). We found that the larger mesoporosity in the 5–100 μm diameter class and macroporosity in the 240–720 μm diameter class reduced the strength of preferential transport. Porosities in these diameter classes were also positively correlated with SOC content (Fig. S5 and S6 and Fukumasu et al., 2022). However, the mesoporosity in the 30–100 μm diameter class, which was the most strongly correlated with the 5 % arrival times, was much more strongly correlated with clay content than with SOC, partly due to the three sandy soils (sand content >65%) that had very large mesoporosities (Fig. S7a,b and Fukumasu et al., 2022), which suggests that any effects of the variations in SOC content (1.1–2.7%) on preferential transport in our field may have been largely overshadowed by the effects of the large variations in clay content (8–42%). It should be noted that when the three sandy soils were removed, the 5% arrival time under 2 mm h^{-1} was weakly but positively correlated with SOC content ($\rho = 0.37$, $P = 0.046$; Fig. S7d), although it was still more strongly and negatively correlated with clay content ($\rho = -0.64$, $P < 0.001$; Fig. S7c). These results also suggest that, compared to soil with smaller clay content, soil with larger clay content would require larger SOC content to achieve similar (i) abundances of small macropores and mesopores (Fukumasu et al., 2022; Soinne et al., 2023), (ii) water flow rates in the soil matrix (as shown by the near-saturated hydraulic conductivity at −6 cm pressure potential; Fig. 10) and (iii) degrees of preferential transport.

Our interpretation on the links between SOC, pore size distribution and solute transport are supported by some previous studies. Earlier, Larsbo et al. (2016) reported positive correlations between SOC content, imaged porosity in the 200–600 μm diameter class and 5% arrival times (i.e. the larger SOC content and imaged porosity, the weaker the preferential transport under steady-state near-saturated flow conditions with 2 mm h^{-1} irrigation intensity) for soil samples having a large variation in SOC contents (4–15%) and relatively constant clay content (ca. 70%). For a Danish arable field with a large variation in topsoil SOC content (1.8–8.4%) and a small variation in clay content (6–14 %), Paradelo et al. (2016) also reported that the larger the SOC content, the weaker the preferential transport under steady-state near-saturated flow conditions with 10 mm h^{-1} irrigation intensity. Additionally, positive associations between SOC content and porosities in the pore diameter ranges 3–1000 μm were reported for arable and grassland soils spanning diverse soil types and textures (e.g. Kirchmann and Gerzabek, 1999; Xu et al., 2018, Jensen et al., 2020; Singh et al., 2020; Soinne et al., 2023; Table S7). Furthermore, Lee et al. (2023) reported that increased SOC content due to land use changes (prairie and switchgrass systems)

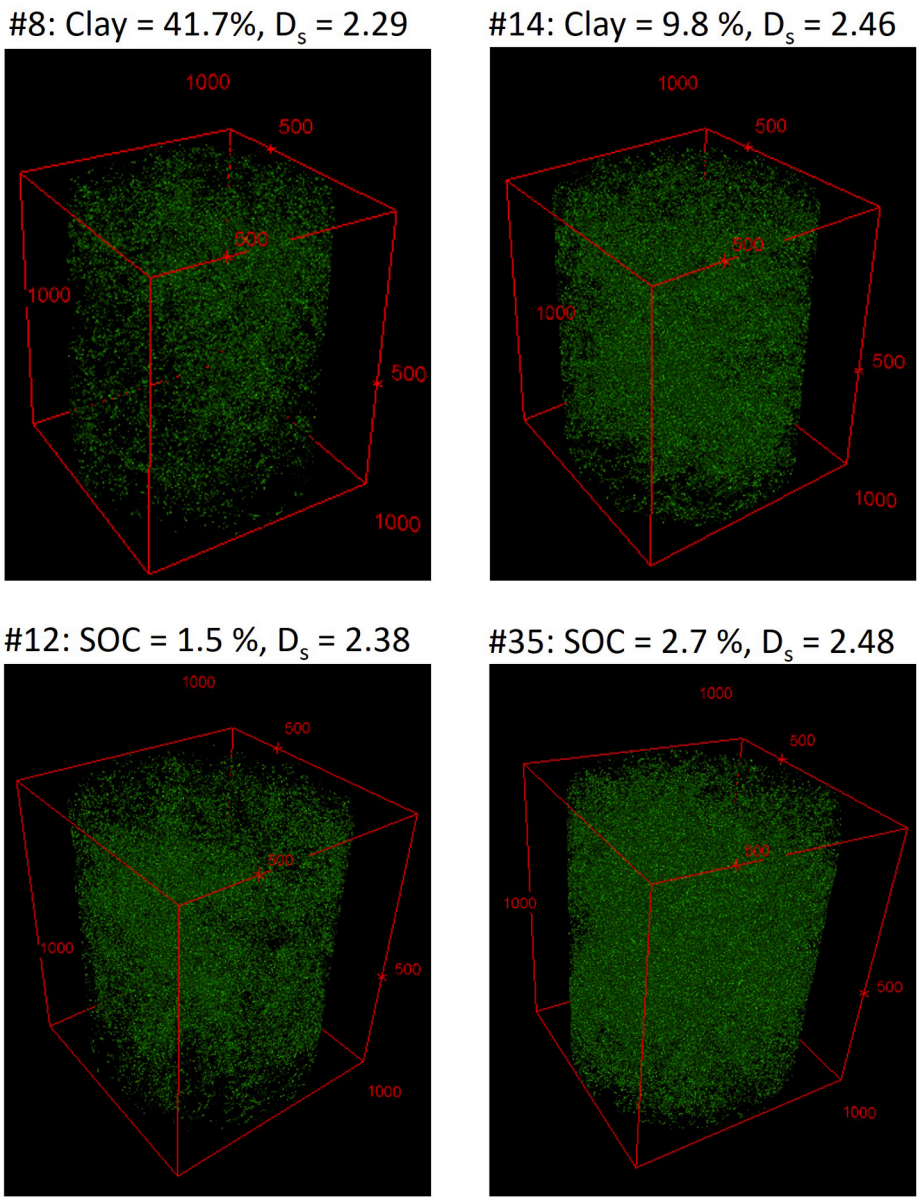

Fig. 11. Examples of imaged pore networks in 240–480 μm diameter size class with samples having contrasting clay content (41.7% vs. 9.8%) and having contrasting SOC content (1.5% vs. 2.7%), while the other properties were similar. D_s is surface fractal dimensions of the whole macropore networks in each sample.

resulted in increased porosity in 50–150 μm diameter class. These studies suggest that an increased SOC content may reduce the risk of preferential transport under near-saturated flow conditions through its effect on the development of denser networks of small macropores and mesopores.

Mechanisms behind the correlations between SOC and the abundances of mesopores and small macropores can be both indirect and direct. For example, the formation of these pores can be induced by biological activity (e.g. fine root growth), which can also increase C input into soil as well as by soil aggregation, which is enhanced with increasing SOC content (Chenu et al., 2000; Meurer et al., 2020a,b; Soinne et al., 2023). In our previous studies, we found that (i) 71–91% of SOC was present in the mineral-associated organic matter (MAOM) fraction, rather than the particulate organic matter (POM) fraction in our soils (Fukumasu et al., 2021), and (ii) total SOC content, which was strongly and positively correlated with SOC in MAOM, was a better predictor for variations in small macropores than SOC in POM (Fukumasu et al., 2022). Likewise, it is well established that a large proportion of SOC is present in the MAOM fraction in the other Swedish arable soils (Simonsson et al., 2014) and in other arable soils globally (e.g. Sokol et al., 2022), even for soils with wide ranges of SOC content (e.g. 0.5–12.0% range for German arable soils (Begill et al., 2023)). These studies suggest that the association between soil fine minerals (i.e. silt- and clay-sized particles) and SOC may be important for soil aggregation and the development of small macropores and mesopores.

It should be noted that the effect of SOC on the degree of preferential transport is dependent on experimental conditions. For example, under initially dry soil conditions, other types of preferential transport mechanisms are possible (Hendrickx and Flury, 2001). Dry soil is often water-repellent and the degree of water repellency is typically positively correlated with SOC content (e.g. Chenu et al., 2000; Hermansen et al., 2019). This implies that larger SOC contents may induce stronger preferential transport under dry soil conditions, either by triggering unstable finger flow or by generating stronger flow in soil macropores (Jarvis et al., 2016). However, the effects of water repellency on preferential transport should be negligible under steady-state near-saturated flow conditions. This notion is supported by previous studies which showed weaker preferential transport with larger SOC contents under

steady-state near-saturated flow conditions (Larsbo et al., 2016; Paradelo et al., 2016).

5. Conclusions

Our study indicated that variation in the strength of preferential solute transport under steady-state near-saturated flow conditions is mostly explained by the abundance of small macropores and mesopores rather than the abundance of larger macropores and their connectivity. In particular, mesoporosity seemed to be important in reducing the degree of preferential transport by connecting small macropores into percolating networks that increase the hydraulic conductivity in the soil matrix, thereby preventing the generation of flow in larger macropores. The effect of soil organic carbon on the degree of preferential transport was limited in our soils, most likely due to a large variation in clay content, which had a much stronger effect on the pore size distribution and near-saturated hydraulic conductivity. However, sequestration of soil organic carbon may potentially reduce the degree of preferential transport under steady-state near-saturated flow conditions because it is positively associated with the abundance of small macropores and mesopores in our soils and in other arable and grassland soils reported in previous studies. It should be noted that the degree of preferential transport is dependent on experimental conditions. Therefore, in future studies, the effects of soil organic carbon on the degree of preferential transport should also be investigated for dry soil conditions, in particular as a consequence of its effects on soil water repellency, which may increase the frequency and strength of preferential flow and transport.

CRediT authorship contribution statement

Jumpei Fukumasu: Writing – review & editing, Writing – original draft, Methodology, Investigation, Formal analysis, Conceptualization. **Nick Jarvis:** Writing – review & editing, Supervision, Methodology, Funding acquisition, Conceptualization. **John Koestel:** Writing – review & editing, Supervision, Methodology. **Mats Larsbo:** Writing – review & editing, Supervision, Resources, Project administration, Methodology, Investigation, Funding acquisition, Conceptualization.

Declaration of competing interest

The authors declare that they have no known competing financial interests or personal relationships that could have appeared to influence the work reported in this paper.

Data availability

Data will be made available on request.

Acknowledgement

This study was financed by FORMAS (grant no: 2016-01320; “Effects of soil organic carbon fractions on soil structure and preferential solute transport”). Soil sampling at Bjertorp was possible thanks to the help from Reza Hosseinpour Ashenaabad and Mattias Gustafsson. We thank Ana Maria Mingot Soriano for the measurements of soil water retention. JF thanks the Heiwa Nakajima Foundation for providing a personal scholarship. We thank Claudia von Brömssen for her advice on the sampling strategy. We thank Tobias Klöffel for proving us with the fitting parameters of X-ray derived pore size distributions. We are grateful to Kjell Carlsson, the manager of the Bjertorp farm, for allowing us to take soil samples.

Appendix A. Supplementary data

Supplementary data to this article can be found online at https://doi.org/10.1016/j.geoderma.2024.117001.

References

Begill, N., Don, A., Poeplau, C., 2023. No detectable upper limit of mineral-associated organic carbon in temperate agricultural soils. Glob. Chang. Biol. 29 (16), 4662–4669. https://doi.org/10.1111/gcb.16804.

Casali, E., Larsbo, M., Koestel, J., Jarvis, N., 2024. Macropore flow in relation to the geometry and topology of soil macropore networks: Re-visiting the kinematic wave equation. J. Hydrol. 630 https://doi.org/10.1016/j.jhydrol.2024.130732.

Chenu, C., Le Bissonnais, Y., Arrouays, D., 2000. Organic matter influence on clay wettability and soil aggregate stability. Soil Sci. Soc. Am. J. 64 (4), 1479–1486. https://doi.org/10.2136/sssaj2000.6441479x.

Chenu, C., Angers, D.A., Barré, P., Derrien, D., Arrouays, D., Balesdent, J., 2019. Increasing organic stocks in agricultural soils: Knowledge gaps and potential innovations. Soil Tillage Res. 188, 41–52. https://doi.org/10.1016/j.still.2018.04.011.

CRC Handbook of Chemistry and Physics, 70th Edition, edited by: Weast, R. C., CRC Press, Boca Raton, FL, USA, p. D-221, 1989.

Demand, D., Blume, T., Weiler, M., 2019. Spatio-temporal relevance and controls of preferential flow at the landscape scale. Hydrol. Earth Syst. Sci. 23 (11), 4869–4889. https://doi.org/10.5194/hess-23-4869-2019.

Dexter, A.R., Richard, G., Arrouays, D., Czyz, E.A., Jolivet, C., Duval, O., 2008. Complexed organic matter controls soil physical properties. Geoderma 144 (3–4), 620–627. https://doi.org/10.1016/j.geoderma.2008.01.022.

Eriksson J., Matsson L., Söderström M., 2010. Tillståndet i svensk åkermark och gröda, data från 2001-2007. (“Current status of Swedish arable soils and cereal crops. Data from 2001-2007”) report 6349. Swedish Environmental Protection Agency, Stockholm, Sweden (In Swedish).

Fu, Z.H., Hu, W., Beare, M., Thomas, S., Carrick, S., Dando, J., Langer, S., Müller, K., Baird, D., Lilburne, L., 2021. Land use effects on soil hydraulic properties and the contribution of soil organic carbon. J. Hydrol. 602 https://doi.org/10.1016/j.jhydrol.2021.126741.

Fukumasu, J., Poeplau, C., Coucheney, E., Jarvis, N., Klöffel, T., Koestel, J., Kätterer, T., Svensson, D.N., Wetterlind, J., Larsbo, M., 2021. Oxalate-extractable aluminum alongside carbon inputs may be a major determinant for organic carbon content in agricultural topsoils in humid continental climate. Geoderma 402. https://doi.org/10.1016/j.geoderma.2021.115345.

Fukumasu, J., Jarvis, N., Koestel, J., Kätterer, T., Larsbo, M., 2022. Relations between soil organic carbon content and the pore size distribution for an arable topsoil with large variations in soil properties. Eur. J. Soil Sci. 73 (1) https://doi.org/10.1111/ejss.13212.

Ghafoor, A., Koestel, J., Larsbo, M., Moeys, J., Jarvis, N., 2013. Soil properties and susceptibility to preferential solute transport in tilled topsoil at the catchment scale. J. Hydrol. 492, 190–199. https://doi.org/10.1016/j.jhydrol.2013.03.046.

Hendrickx, J.M., and Flury, M. 2001. Uniform and preferential flow mechanisms in the vadose zone. Conceptual Models of Flow and Transport in the Fractured Vadose Zone, National Academy Press, Washington D.C: 149–187.

Hermansen, C., Moldrup, P., Müller, K., Jensen, P.W., van den Dijssel, C., Jeyakumar, P., de Jonge, L.W., 2019. Organic carbon content controls the severity of water repellency and the critical moisture level across New Zealand pasture soils. Geoderma 338, 281–290. https://doi.org/10.1016/j.geoderma.2018.12.007.

Horn, R., Taubner, H., Wuttke, M., Baumgartl, T., 1994. Soil physical-properties related to soil-structure. Soil Tillage Res. 30 (2–4), 187–216. https://doi.org/10.1016/0167-1987(94)90005-1.

Jarvis, N.J., 2007. A review of non-equilibrium water flow and solute transport in soil macropores: principles, controlling factors and consequences for water quality. Eur. J. Soil Sci. 58 (3), 523–546. https://doi.org/10.1111/j.1365-2389.2007.00915.x.

Jarvis, N., Koestel, J., Messing, I., Moeys, J., Lindahl, A., 2013. Influence of soil, land use and climatic factors on the hydraulic conductivity of soil. Hydrol. Earth Syst. Sci. 17 (12), 5185–5195. https://doi.org/10.5194/hess-17-5185-2013.

Jarvis, N., Koestel, J., Larsbo, M., 2016. Understanding Preferential Flow in the Vadose Zone: Recent Advances and Future Prospects. Vadose Zone J. 15 (12) https://doi.org/10.2136/vzj2016.09.0075.

Jarvis, N., Larsbo, M., Koestel, J., 2017a. Connectivity and percolation of structural pore networks in a cultivated silt loam soil quantified by X-ray tomography. Geoderma 287, 71–79. https://doi.org/10.1016/j.geoderma.2016.06.026.

Jarvis, N., Forkman, J., Koestel, J., Kätterer, T., Larsbo, M., Taylor, A., 2017b. Long-term effects of grass-clover leys on the structure of a silt loam soil in a cold climate. Agr Ecosyst Environ 247, 319–328. https://doi.org/10.1016/j.agee.2017.06.042.

Jarvis, N.J., Moeys, J., Koestel, J., Hollis, J.M., 2012. Preferential Flow in a Pedological Perspective. In: Hydropedology: Synergistic Integration of Soil Science and Hydrology, pp. 75–120. https://doi.org/10.1016/b978-0-12-386941-8.00003-4.

Jensen, J.L., Schjonning, P., Watts, C.W., Christensen, B.T., Munkholm, L.J., 2020. Short-term changes in soil pore size distribution: Impact of land use. Soil Tillage Res. 199, 104597 https://doi.org/10.1016/j.still.2020.104597.

Johannes, A., Matter, A., Schulin, R., Weisskopf, P., Baveye, P.C., Boivin, P., 2017. Optimal organic carbon values for soil structure quality of arable soils. Does clay content matter? Geoderma 302, 14–21. https://doi.org/10.1016/j.geoderma.2017.04.021.

Karup, D., Moldrup, P., Paradelo, M., Katuwal, S., Norgaard, T., Greve, M.H., de Jonge, L.W., 2016. Water and solute transport in agricultural soils predicted by volumetric clay and silt contents. J. Contam. Hydrol. 192, 194–202. https://doi.org/10.1016/j.jconhyd.2016.08.001.

Katuwal, S., Norgaard, T., Moldrup, P., Lamandé, M., Wildenschild, D., de Jonge, L.W., 2015. Linking air and water transport in intact soils to macropore characteristics inferred from X-ray computed tomography. Geoderma 237, 9–20. https://doi.org/10.1016/j.geoderma.2014.08.006.

Kirchmann, H., Gerzabek, M.H., 1999. Relationship between soil organic matter and micropores in a long-term experiment at Ultuna, Sweden. J. Pllant Nutr. Soil Sci. 162 (5), 493–498. https://doi.org/10.1002/(SICI)1522-2624(199910)162:5<493::AID-JPLN493>3.0.CO;2-S.

Knudby, C., Carrera, J., 2005. On the relationship between indicators of geostatistical, flow and transport connectivity. Adv. Water Resour. 28 (4), 405–421. https://doi.org/10.1016/j.advwatres.2004.09.001.

Koestel, J., 2018. SoilJ: An ImageJ Plugin for the Semiautomatic Processing of Three-Dimensional X-ray Images of Soils. Vadose Zone J. 17 (1) https://doi.org/10.2136/vzj2017.03.0062.

Koestel, J., Larsbo, M., 2014. Imaging and quantification of preferential solute transport in soil macropores. Water Resour. Res. 50 (5), 4357–4378. https://doi.org/10.1002/2014wr015351.

Koestel, J., Dathe, A., Skaggs, T.H., Klakegg, O., Ahmad, M.A., Babko, M., Giménez, D., Farkas, C., Nemes, A., Jarvis, N., 2018. Estimating the Permeability of Naturally Structured Soil From Percolation Theory and Pore Space Characteristics Imaged by X-Ray. Water Resour. Res. 54 (11), 9255–9263. https://doi.org/10.1029/2018wr023609.

Koestel, J., Larsbo, M., Jarvis, N., 2020. Scale and REV analyses for porosity and pore connectivity measures in undisturbed soil. Geoderma 366. https://doi.org/10.1016/j.geoderma.2020.114206.

Koestel, J.K., Moeys, J., Jarvis, N.J., 2011. Evaluation of Nonparametric Shape Measures for Solute Breakthrough Curves. Vadose Zone J. 10 (4), 1261–1275. https://doi.org/10.2136/vzj2011.0010.

Koestel, J.K., Moeys, J., Jarvis, N.J., 2012. Meta-analysis of the effects of soil properties, site factors and experimental conditions on solute transport. Hydrology and Earth System Sciences 16 (6), 1647–1665. https://doi.org/10.5194/hess-16-1647-2012.

Kosugi, K., 1994. Three-parameter lognormal-distribution model for soil-water retention. Water Resour. Res. 30 (4), 891–901. https://doi.org/10.1029/93wr02931.

Langner, H.W., Gaber, H.M., Wraith, J.M., Huwe, B., Inskeep, W.P., 1999. Preferential flow through intact soil cores: Effects of matric head. Soil Sci. Soc. Am. J. 63 (6), 1591–1598. https://doi.org/10.2136/sssaj1999.6361591x.

Larsbo, M., Koestel, J., Jarvis, N., 2014. Relations between macropore network characteristics and the degree of preferential solute transport. Hydrol. Earth Syst. Sci. 18 (12), 5255–5269. https://doi.org/10.5194/hess-18-5255-2014.

Larsbo, M., Koestel, J., Kötterer, T., Jarvis, N., 2016. Preferential Transport in Macropores is Reduced by Soil Organic Carbon. Vadose Zone J. 15 (9) https://doi.org/10.2136/vzj2016.03.0021.

Lee, J.H., Lucas, M., Guber, A.K., Li, X.F., Kravchenko, A.N., 2023. Interactions among soil texture, pore structure, and labile carbon influence soil carbon gains. Geoderma 439. https://doi.org/10.1016/j.geoderma.2023.116675.

Lucas, M., Schlüter, S., Vogel, H.J., Vetterlein, D., 2019. Soil structure formation along an agricultural chronosequence. Geoderma 350, 61–72. https://doi.org/10.1016/j.geoderma.2019.04.041.

Luo, L.F., Lin, H., Schmidt, J., 2010. Quantitative Relationships between Soil Macropore Characteristics and Preferential Flow and Transport. Soil Sci. Soc. Am. J. 74 (6), 1929–1937. https://doi.org/10.2136/sssaj2010.0062.

Meurer, K., Barron, J., Chenu, C., Coucheney, E., Fielding, M., Hallett, P., Herrmann, A. M., Keller, T., Koestel, J., Larsbo, M., Lewan, E., Or, D., Parsons, D., Parvin, N., Taylor, A., Vereecken, H., Jarvis, N., 2020a. A framework for modelling soil structure dynamics induced by biological activity. Glob. Chang. Biol. 26 (10), 5382–5403. https://doi.org/10.1111/gcb.15289.

Meurer, K.H.E., Chenu, C., Coucheney, E., Herrmann, A.M., Keller, T., Kätterer, T., Nimblad Svensson, D., Jarvis, N., 2020b. Modelling dynamic interactions between soil structure and the storage and turnover of soil organic matter. Biogeosciences 17 (20), 5025–5042. https://doi.org/10.5194/bg-17-5025-2020.

Mori, Y., Higashi, N., 2009. Controlling solute transport processes in soils by using dual-porosity characteristics of natural soils. Colloids and Surfaces a-Physicochemical and Engineering Aspects 347 (1–3), 121–127. https://doi.org/10.1016/j.colsurfa.2009.02.009.

Mori, Y., Maruyama, T., Mitsuno, T., 1999. Soft x-ray radiography of drainage patterns of structured soils. Soil Sci. Soc. Am. J. 63 (4), 733–740. https://doi.org/10.2136/sssaj1999.634733x.

Nimmo, J.R., 2021. The processes of preferential flow in the unsaturated zone. Soil Sci. Soc. Am. J. 85 (1), 1–27. https://doi.org/10.1002/saj2.20143.

Oldfield, E.E., Bradford, M.A., Wood, S.A., 2019. Global meta-analysis of the relationship between soil organic matter and crop yields. Soil 5 (1), 15–32. https://doi.org/10.5194/soil-5-15-2019.

Paradelo, M., Katuwal, S., Moldrup, P., Norgaard, T., Herath, L., de Jonge, L.W., 2016. X-ray CT-Derived Soil Characteristics Explain Varying Air, Water, and Solute Transport Properties across a Loamy Field. Vadose Zone J. 15 (4) https://doi.org/10.2136/vzj2015.07.0104.

Rabot, E., Wiesmeier, M., Schlüter, S., Vogel, H.J., 2018. Soil structure as an indicator of soil functions: A review. Geoderma 314, 122–137. https://doi.org/10.1016/j.geoderma.2017.11.009.

Renard, P., Allard, D., 2013. Connectivity metrics for subsurface flow and transport. Adv. Water Resour. 51, 168–196. https://doi.org/10.1016/j.advwatres.2011.12.001.

Sammartino, S., Lissy, A.S., Bogner, C., Van den Bogaert, R., Capowiez, Y., Ruy, S., Cornu, S., 2015. Identifying the Functional Macropore Network Related to Preferential Flow in Structured Soils. Vadose Zone J. 14 (10) https://doi.org/10.2136/vzj2015.05.0070.

Sandin, M., Koestel, J., Jarvis, N., Larsbo, M., 2017. Post-tillage evolution of structural pore space and saturated and near-saturated hydraulic conductivity in a clay loam soil. Soil Tillage Res. 165, 161–168. https://doi.org/10.1016/j.still.2016.08.004.

Sandin, M., Piikki, K., Jarvis, N., Larsbo, M., Bishop, K., Kreuger, J., 2018. Spatial and temporal patterns of pesticide concentrations in streamflow, drainage and runoff in a small Swedish agricultural catchment. Sci. Total Environ. 610, 623–634. https://doi.org/10.1016/j.scitotenv.2017.08.068.

Schindelin, J., Arganda-Carreras, I., Frise, E., Kaynig, V., Longair, M., Pietzsch, T., Preibisch, S., Rueden, C., Saalfeld, S., Schmid, B., Tinevez, J.Y., White, D.J., Hartenstein, V., Eliceiri, K., Tomancak, P., Cardona, A., 2012. Fiji: an open-source platform for biological-image analysis. Nat. Methods 9 (7), 676–682. https://doi.org/10.1038/nmeth.2019.

Schlüter, S., Albrecht, L., Schwärzel, K., Kreiselmeier, J., 2020. Long-term effects of conventional tillage and no-tillage on saturated and near-saturated hydraulic conductivity - Can their prediction be improved by pore metrics obtained with X-ray CT? Geoderma 361. https://doi.org/10.1016/j.geoderma.2019.114082.

Simonsson, M., Kirchmann, H., Magid, J., Kätterer, T., 2014. Can Particulate Organic Matter Reveal Emerging Changes in Soil Organic Carbon? Soil Sci. Soc. Am. J. 78 (4), 1279–1290. https://doi.org/10.2136/sssaj2013.12.0533.

Singh, J., Singh, N., Kumar, S., 2020. X-ray computed tomography-measured soil pore parameters as influenced by crop rotations and cover crops. Soil Sci. Soc. Am. J. 84 (4), 1267–1279. https://doi.org/10.1002/saj2.20105.

Soares, A., Moldrup, P., Vendelboe, A.L., Katuwal, S., Norgaard, T., Delerue-Matos, C., Tuller, M., de Jonge, L.W., 2015. Effects of Soil Compaction and Organic Carbon Content on Preferential Flow in Loamy Field Soils. Soil Sci. 180 (1), 10–20. https://doi.org/10.1097/ss.0000000000000105.

Soinne, H., Keskinen, R., Tähtikarhu, M., Kuva, J., Hyväluoma, J., 2023. Effects of organic carbon and clay contents on structure-related properties of arable soils with high clay content. Eur. J. Soil Sci. 74 (5) https://doi.org/10.1111/ejss.13424.

Sokol, N., Whalen, E.D., Jilling, A., Kallenbach, C., Pett-Ridge, J., Georgiou, K., 2022. Global distribution, formation and fate of mineral-associated soil organic matter under a changing climate: A trait-based perspective. Funct. Ecol. 36 (6), 1411–1429. https://doi.org/10.1111/1365-2435.14040.

Vendelboe, A.L., Schjonning, P., de Jonge, L.W., Moldrup, P., 2013. Long-Term Effect of Different Carbon Management Strategies on Water Flow and Related Processes for Three Loamy Soils. Soil Sci. 178 (8), 379–388. https://doi.org/10.1097/ss.0000000000000011.

Vogel, H.J., 2000. A numerical experiment on pore size, pore connectivity, water retention, permeability, and solute transport using network models. Eur. J. Soil Sci. 51 (1), 99–105. https://doi.org/10.1046/j.1365-2389.2000.00275.x.

Xu, L.Y., Wang, M.Y., Shi, X.Z., Yu, Q.B., Shi, Y.J., Xu, S.X., Sun, W.X., 2018. Effect of long-term organic fertilization on the soil pore characteristics of greenhouse vegetable fields converted from rice-wheat rotation fields. Sci. Total Environ. 631–632, 1243–1250. https://doi.org/10.1016/j.scitotenv.2018.03.070.

Zhang, Z.B., Liu, K.L., Zhou, H., Lin, H., Li, D.M., Peng, X.H., 2019. Linking saturated hydraulic conductivity and air permeability to the characteristics of biopores derived from X-ray computed tomography. J. Hydrol. 571, 1–10. https://doi.org/10.1016/j.jhydrol.2019.01.041.